INKJET-PRINTED CONDUCTIVE FEATURES FOR RAPID INTEGRATION OF ELECTRONIC CIRCUITS IN CENTRIFUGAL MICROFLUIDICS

J. Kruger[1], S. Smith[2], K. Land[3], M. du Plessis[4] & T-H. Joubert[5]*

[1]Department of Electrical, Electronic and Computer Engineering,
University of Pretoria, South Africa
u10066081@tuks.co.za

[2]Department of Material Science and Manufacturing,
Council of Scientific and Industrial Research, South Africa
SSmith@csir.co.za

[3]Department of Material Science and Manufacturing,
Council of Scientific and Industrial Research, South Africa
KLand@csir.co.za

[4]Department of Electrical, Electronic and Computer Engineering,
University of Pretoria, South Africa
monuko@up.co.za

[5]Department of Electrical, Electronic and Computer Engineering,
University of Pretoria, South Africa
trudi.joubert@up.co.za

ABSTRACT

This work investigates the properties of conductive circuits inkjet-printed onto the polycarbonate discs used in CD-based centrifugal microfluidics, contributing towards rapidly prototyped electronic systems in smart ubiquitous biosensors, which require sensitive and robust signal readout at low power and cost, and with wireless connectivity. A protocol for inkjet-printing electronic networks on CD substrates is developed. The circuit modeling of conductive tracks is discussed, and validated against experimental results. A design procedure is presented for reliably printing conductive networks with feature dimensions between 150 µm and 2 mm on CDs, and yielding electronic circuits operating with a bandwidth of 1 MHz.

Keywords: printed electronics, conductive inks, circuit model, centrifugal microfluidics, rapid prototyping, smart sensing

OPSOMMING

---

[1] The author was enrolled for an B Eng (Electronic) degree in the Department of Electrical, Electronic and Computer Engineering, University of Pretoria

[2] The author was a senior engineer in the Department of Material Science and Manufacturing, Council of Scientific and Industrial Research

[3] The author was the group leader in the Department of Material Science and Manufacturing, Council of Scientific and Industrial Research

[4] The author was a professor in the Department of Electrical, Electronic and Computer Engineering, University of Pretoria

[5] The author was a senior lecturer in the Department of Electrical, Electronic and Computer Engineering, University of Pretoria

*Corresponding author

Hierdie werk ondersoek die eienskappe van inkstraal-gedrukte geleidende stroombane op polikarbonaatskywe wat in kompakskyf-gebaseerde sentrifugale mikrovloeistelsels gebruik word, en dra by tot snel-geprototipeerde elektroniese stelsels in intelligente alomteenwoordige biosensors wat sensitiewe en robuuste seinuitlees vereis teen lae koste en drywing, en met koordlose kommunikasie. 'n Protokol vir die inkstraal-druk van elektroniese netwerke op kompakskyfsubstrate is ontwikkel. Die stroombaanmodelering van geleidende lyne word bespreek, en teen eksperimentele resultate bevestig. 'n Ontwerpsprosedure word voorgehou vir betroubare druk van geleidende netwerke met struktuurdimensies tussen 150 µm en 2 mm op kompakskywe, wat elektroniese netwerke lewer wat in 'n bandwydte van 1 MHz funksioneer.

Sleutelwoorde: gedrukte elektronika, geleidende ink, stroombaanmodel, sentrifugale mikrovloeistelsel, snelle prototipering, intelligente deteksie

1. INTRODUCTION

Applications in diagnostic point-of-care and agricultural or environmental point-of-need must adhere to the ASSURED principles of the World Health Organization - Affordable, Sensitive, Specific, User-friendly, Rapid and Robust, Equipment-free, Deliverable to end-users. ASSURED compliance requires the development of processes and building blocks to add smart features to disposable biosensors on low-cost substrates.

Microfluidics provide promising techniques in the field of low-cost point-of-care testing [1]. Examples of microfluidic devices are shown in Figure 1, ranging from simple paper-based lateral flow devices to more complex hybrid systems. The general intention is that microfluidic devices manipulate small volumes of samples, with low requirements for size and reagents - both of which are expensive. Fluidic control is required for accurate testing, and therefore most microfluidic devices rely on valves, pumps and other flow control mechanisms. Despite the excellent functionality presented by microfluidics, fabrication requiring clean room facilities still presents cost and time barriers to the widespread use of these devices outside of laboratories [2]. Additionally, microfluidic systems requiring bulky, expensive pumping mechanisms for fluidic handling are not favourable for point-of-care applications.

The lab-on-a-disc technology, also known as centrifugal microfluidics, is proposed to circumvent these application barriers, and is well-suited to the development of point-of-care diagnostics [3]. Centrifugal microfluidic discs can be designed in two-dimensional layers and can be rapidly prototyped to produce microfluidic devices with complex functionality with turnaround times of a few hours - from concept to fully operational devices. Low cost polycarbonate materials are commonly used to fabricate centrifugal microfluidic disc devices along with adhesive layers to bind multiple fluidic layers. The technologies to design and manufacture them are also widely available and affordable, for example razor cutting and laser machining. Polycarbonate can also be injection-molded, which makes it appropriate for the mass production of inexpensive devices. Furthermore, minimal instrumentation is required to drive the disc and facilitate fluidic functionality - only a small motor is required to spin the disc and create the centrifugal forces which allow for fluidic manipulation.

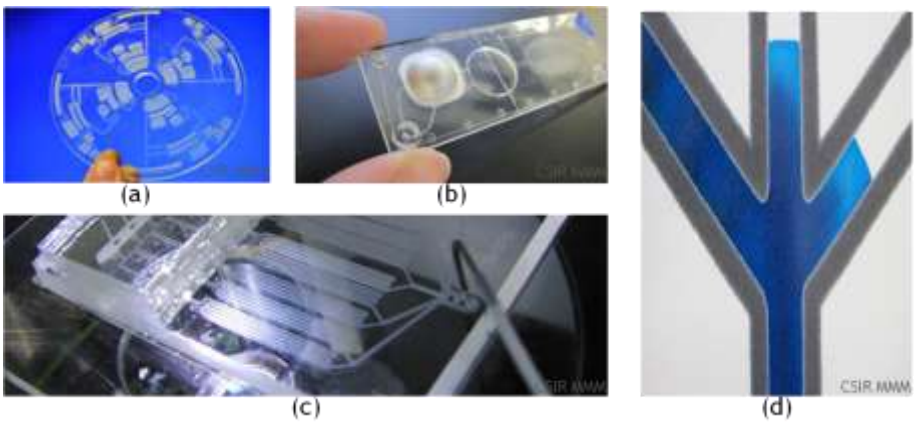

Figure 1 Examples of microfluidic devices: (a) centrifugal CD disc, (b) hybrid integrated system, (c) soft lithography in PDMS, (d) wax on paper

While microfluidics provide promising techniques in the field of low cost point-of-care applications, co-integration with electronics and optics may add powerful intelligence to systems [4][5][6] - as long as this can be accomplished within size and cost constraints.

Printed electronics has application in providing low-cost biosensors, because it allows for disposable components such as sensor electrodes to be realized [7][8]. As an additive technique, printing allows the manufacturing of electronic circuits with efficient use of expensive materials and minimal waste, which is also ecologically friendly. Printed electronics is an attractive emerging field, and is an active area of research and development globally. Several printing technologies are utilized, ranging from screen-printing for thick film larger feature structures to gravure printing for mass production of printed electronic devices. Rapid prototyping of electronic circuit designs is achievable using inkjet-printable inorganic nanoparticle solutions to form conductive circuit networks, enabling smart sensor systems to be developed and implemented on unusual substrates [4][5][6].

In summary, this work investigates the properties of conductive circuits inkjet-printed onto the polycarbonate compact discs (CDs) used in CD-based centrifugal microfluidics:

- A protocol for high resolution printing of electronic networks on CD substrates is developed, including investigations on material properties of the substrate and conductive ink and the manufacturing processes associated with inkjet-printed electronics.
- The electrical parameters of interest for conductive network tracks are resistance, as well as the parasitic inductance and capacitance [9]. The circuit parameter modeling of printed electronic components is discussed, and the ensuing circuit model is validated against experimental results in the physical and electrical domain. The emphasis of this work is on the resistance of the conductive tracks, while the inductance and capacitance are only considered as factors limiting the practical frequency range of the printed electronics circuits.
- A systematic design procedure based on sheet resistance is presented for reliably printing conductive networks with feature dimensions between 100 µm and 2 mm onto microfluidic CDs. It is confirmed that the ensuing printed structures yield electronic circuit networks operating with a bandwidth of at least 1 MHz - a practical target value for CD-based lab-on-a-disc printed electronics systems.

2. MANUFACTURING PROCESS

Inkjet printing is a continuous non-contact digital printing technique. The most common types of inkjet printing are thermal and piezoelectric, both of which fall into the category of drop-on-demand printing. The printer deposits droplets of functional solutions through a micrometer sized nozzle onto the substrate. Typical substrates and inks used in printed electronics are summarised in Table 1.

Table 1: Typical materials used for printed electronics

Substrates	*Inks*
• Paper	• Carbon
• Glass	• Silver
• Polyimide (PI)	• Gold
• Polyethylene terephthalate (PET)	• Platinum
• Polydimethylsiloxane (PDMS)	• Titanium
• Polycarbonate (PC)	• Conductive polymers (notably PEDOT:PSS)
• Poly (methyl methacrylate) (PMMA)	• Dielectric materials

In the inkjet printing manufacturing process for this work, the standard commercial products shown in Figure 2 are employed, using default recommended settings as far as possible. Single-layer conductive track samples are fabricated with a Dimatix DMP-3281 materials deposition printer using Harima NPS-J nanosilver ink, followed by thermal sintering in an oven, as recommended by the ink manufacturer.

The Fujifilm Dimatix DMP-3281 is a drop-on-demand piezo inkjet printer with a 5 µm mechanical resolution that allows multi-layer printing onto an A4-sized heatable platen. The printing cartridge has 16 nozzles, each with a 21 µm orifice furnishing a minimum 10 pl

drop volume. The printing resolution of the inkjet process using this machine is mainly governed by the nozzle diameter (approximately the droplet diameter) and the statistical variation of the droplet flight and spreading on the substrate.

As discussed in [9], the typical solution processable inorganic conductive printed electronics ink is a colloidal solvent suspension of metal nanoparticles encapsulated in a resin binder, often also containing electrically active dispersants or other surfactants to avoid settling and agglomeration, and humectants to control the evaporation rate. Silver nano-ink is the most ubiquitous and cost-effective inorganic conductive ink [10]. The Harima NPS-J ink contains 12 nm silver particles, in the non-polar tetradecane solvent at a 64 wt% loading. This low-viscosity paste (9 cP) provides good inkjet printability and excellent adhesion when applied on a variety of substrates.

(a) (b) (c)

Figure 2 Commercial inkjet printing products (a) Harima NPS-J nanosilver ink, (b) 10pl drop volume print head with ink cartridge, (c) Fujifilm Dimatix DMP-3281printer

Polycarbonate (PC) is used in the electronics industry as inductor body material, particularly in audio applications. A summary of the properties of PC is provided in Table 2. PC is inherently hydrophobic - the contact angle of water on unmodified PC is 84° [11]. PC is electrostatically active, and has a low surface energy of 42 mJ/m^2 and poor polarizability, meaning that typical inkjet-printable inks cannot bond with the surface. Surface cleaning and chemical activation is therefore a critical prerequisite to improve wetability of the substrate surface to the ink. Wiping or washing with a solvent cleans loose particles and degreases the surface, while also increasing the surface energy. Solvents such as methanol or isopropanol are acceptable for PC (while acetone is not). PC is compatible with a wide range of organic oils, including the tetradecane solvent of the Harima NPS-J nanosilver ink.

Table 2: Properties of polycarbonate

Physical		***Processing***	
Specific gravity	1.2 g/cc	Alcohols	Acceptable
Water absorption	0.2%	Weak acids	Acceptable
Surface energy	42 mJ/m^2	Weak alkalis	Acceptable
Contact angle of water	84°	Organic oils	Acceptable
Thermal		***Electrical***	
Melting temperature	155°C	Surface resistivity	$1X10^{13}$ Ω/□
Glass transition temperature	147°C	Volume resistivity	$1X10^{12}$ Ω-m
Upper working temperature	130°C	Dielectric constant	2.99 @ 1MHz
Thermal conductivity	0.187 W/ m·K	Relative permeability	0.866 @ 1 MHz
Thermal expansion coefficient	$70x10^{-6}$/K	Dissipation factor	0.0009

When printing the Harima nanosilver ink onto pretreated PC CDs with the Dimatix printing parameters shown in Table 3, the obtainable printed spot diameter is approximately 80 μm. This spot size is larger than the 50 μm spot obtained for Epson photo paper [9], which is recommended as a standard printed electronics substrate for the Dimatix printer.

Table 3: Dimatix printing parameters (single nozzle).

Parameter	*Setting*
Waveform	Dimatix model fluid double pulse(for low viscosity ink)
Jetting voltage	28 V
Meniscus point	3.5 (relative to water)
Nozzle temperature	30 °C
Platen temperature	50 °C
Cartridge height	1 mm
Drop spacing	25 μm

The post-printing thermal curing process evaporates the carrier solvent, and at the silver nanoparticle sintering temperature conductivity is achieved as a result of point-to-point contact between the silver particles. Even higher temperatures decompose residual non-conductive binders, and increase the conductivity of the printed structure. The recommended thermal curing for the Harima NPS-J nanosilver ink (on a PET substrate) is at a temperature of 220°C for 60 minutes. The resultant silver film is 4 μm thick with a specific resistance of 3 μΩ·cm. The density difference between a nanosilver layer and bulk silver leads to a decreased conductivity of the printed layer with respect to bulk. Thin printed films permit uniform sintering, creating better conductivity for electronic tracks.

High processing temperatures, however, can be detrimental to the substrate material causing it to melt, crack, warp, weaken and discolour. Adhesion between the substrate and the conductive layer is also affected by high temperature, and the printed tracks may delaminate. PC is sensitive to temperature and requires lower thermal processing at temperatures of maximum 130°C. In this case the residual binders limit the achievable conductivity. From experimentation, sintering at a temperature of 130°C for 2 hours yields satisfactory results.

For a workflow enabling the attainment of successful conductive structure printing on polycarbonate CDs, the following manufacturing process conditions are considered important: (i) substrate preparation, (ii) jetting parameters, (iii) platen temperature, (iv) sintering temperature profile and time.

i. Substrate preparation
   - The substrate is cleaned with isopropanol alcohol.
   - The substrate is dried by blowing with compressed air (or nitrogen).

ii. The electrical structures were immediately printed on the pretreated substrate.
   - The jetting parameters are set using the Dimatix drop watcher application, and the values in Table 3 generally agree with those for a low viscosity ink.
   - Setting the platen temperature provides control over the spreading of ink on the substrate, which needed to be limited on the pretreated substrates. Increasing the platen temperature also improves adhesion of the printed structures to the CD.

iii. The printed structures was cured in a laboratory oven.
   - The highest PC working temperature of 130°C is used to maximize the nanoparticle sintering.
   - The most efficient thermal profile is sintering for 2 hours in a preheated oven and then leaving the structures in the cooling oven till room temperature is reached.

3. EXPERIMENTAL STUCTURES

3.1 Layout design

Similarly to the discussion in [9] for conductive networks printed on paper, the electrical parameters of interest for tracks are track resistance, as well as the parasitic inductance

and capacitance. Kelvin probing [12], where a low impedance outer loop drives current through a sample while the voltage drop is measured on an inner loop, is commonly used to reduce positive measurement errors from contact and lead resistance.

The “dogbone” layout configuration is chosen for the test structures, since the straight lines are best to keep the cross sectional area as constant as possible. The parallel field lines of a feature where the line length is larger than the width avoids current crowding [12], and reduces positive errors due to increased current density at the probe points. The probe pad dimensions of 2 mm × 2mm match the size of the instrument probe connector. Several line widths between 150 µm and 2 mm are used, and each line consists of three identical track elements. The pad pitch of 8 mm presents an adequate aspect ratio for the largest line width. Figure 3 shows the layout design of the test structures.

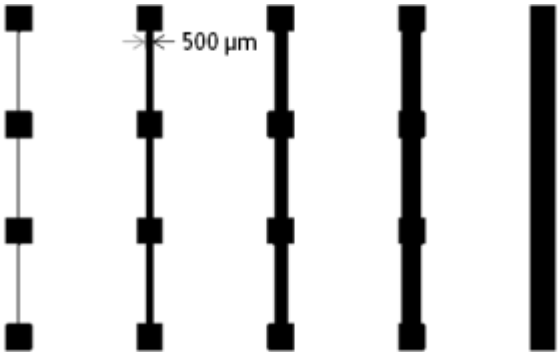

Figure 3 3-Element dogbone layout with line width varying between 150 µm and 2mm

3.2 Electrical model

The equivalent electrical circuit of a conductive line is approximated with lumped components in the model of Figure 4 (a). Z is a measurable complex frequency dependent impedance, with the real part equivalent to the line resistance R, while the capacitance C and the inductance L contribute to the imaginary reactance X. The value of R is independent of frequency, while the value of X is a function of frequency. If the L contributes a dominant pole a high pass frequency response will ensue, while if the dominant pole is contributed by the C a low pass frequency response will ensue. In this model the R and L are inherent in single printed line, while the C is associated with gaps between parallel printed lines, or between a printed line and a ground plane.

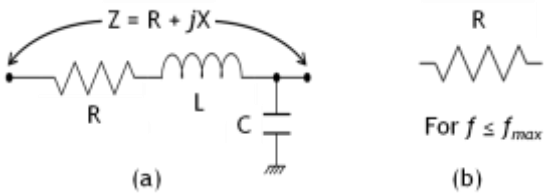

Figure 4 (a) Lumped impedance model and (b) limited bandwidth resistor model

The equations in Table 4 govern the lumped component values in the impedance model for planar lines with a rectangular cross section, which is a plausible approximation for inkjet-printed lines with dimensions as defined in Figure 5. The parameters for the equations are as follows:

- *t:* thickness of the line (m)
- w*:* width of the line (m)
- *l*: length of the line (m)
- *d*: distance between parallel printed lines, or a line and a ground plane (m)

- A_l: cross sectional area along the length of the line (m^2)
- A_s: cross sectional area of the line side wall (m^2)
- ρ: conductive material resistivity (Ω·m)
- ε: dielectric material (composite of air and polycarbonate) permittivity (F/m)
- $f_{c\text{-}HP}$: -3 dB high pass cut-off frequency for series L-R network (Hz)
- $f_{c\text{-}LP}$: -3 dB low pass cut-off frequency for series R-C network (Hz)

Table 4: Model component equations for rectangular planar lines

Model component equation	Reference
(1) $R = \rho \times l / A_l = \rho \times l / (w \times t)$	[13]
(2) $L = 0.2 \times l \times (\ln(2 \times l/(w+t)) + ½ + 0.2235 \times (w+t)/l)$	[14]
(3) $C = \varepsilon \times A_s / d = \varepsilon \times (l \times t) / d$	[13]
(4) $f_{c\text{-}HP} = BW_{HP} = R/2\pi L$	[15]
(5) $f_{c\text{-}HP} = BW_{LP} = 1/2\pi RC$	[15]

The circuit model may be reduced to the purely resistive one of Figure 4 (b) when the frequency of circuit operation is within the frequency range defined by the bandwidth of the Figure 4 (a) impedance. In particular, for a single conductive line far away from other conductive lines or planes, C may be neglected, while L may be neglected for frequencies within the limited bandwidth. For printed conductive lines in general, the high-pass impedance spectrum is dominated by the series track inductance L [9], and the highest frequency of circuit operation is consequently determined by R and L.

A resistance metric often used in microlectronics design for films with uniform thickness, is the sheet resistance R_{sh}, which simplifies network design procedures. The definition of sheet resistance is detailed in Figure 5 as the resistance of a square of the film material - independent of the square dimensions - with units of Ohms-per-square (Ω/□). The dimensions of any line of the same material may then be designed as the number of squares necessary to implement the desired resistance R.

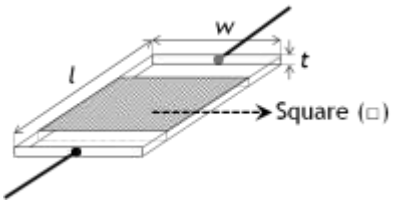

Figure 5 Sheet resistance as design metric : R = ρ / t = Rsh ▫ #□

In order to extract the sheet resistance as a potential design metric for conductive silver lines inkjet-printed onto polycarbonate CDs, measurement of the dimensions of the printed features is required, in addition to the electrical measurements.

4. EXPERIMENTAL RESULTS

A qualitative visual appraisal of the printed dogbone structures in Figure 6 indicates feature shapes that are well defined and adherent on the substrate, while edge raggedness is noticeable on the widest line. There appears to be a "coffee-ring" effect where the edges of shapes are thicker than the central parts of the features - this is particularly evident on the probe pads. The origin of this effect is most probably related to uneven sintering caused by the temperature gradient created across the thickness of the printed layer by the difference in the thermal conductivity of polycarbonate (0.187 W/m·K) relative to that of air (0.024 W/m·K). Improvement of the "coffee-ring" effect calls for further investigation.

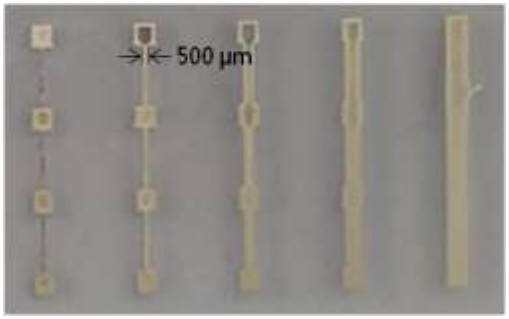

Figure 6 Silver inkjet-printed dogbone structures on polycarbonate CD substrate with line width varying between 150 µm and 2mm

4.1 Measurement setup

A Zeiss LSM5 confocal microscope set up for 0.5 µm slices is used to measure the feature dimensions via laser profilometry. The roughness or flatness of the substrate affects measurements for thin layers, yielding 1 µm as the lower limit of resolution without excessive noise and errors.

The GW-Instek 8110 LCR 4-point probe routes the inner and outer loops to the same points on a pair of connectors, so that a two-pad layout design can be used with a custom spring-loaded (pogo) pin setup to perform 4-point Kelvin probing. A wideband calibration mode on the instrument is used to adjust for the wire and contact impedance of the leads, crocodile clips and pogo pins. To compensate for inconsistency in pogo pin contact with the probe pads, each measurement was repeated three times and the average value was used as the result.

The equipment and measurement jig used during the characterization of the printed dogbone structures is shown in Figure 7.

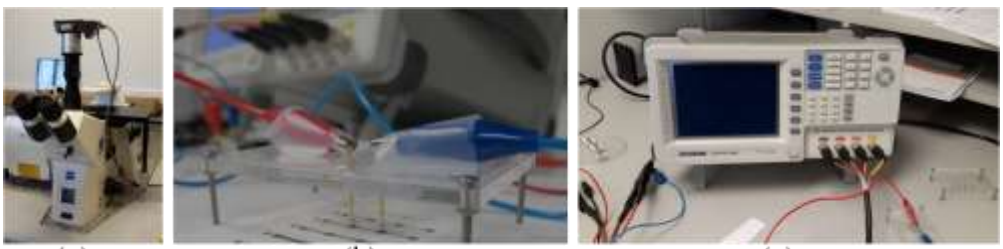

Figure 7 Measurement setup (a) Zeiss LSM 5 Pascal confocal microscope (b) spring-loaded pin measurement jig (c) GW-Instek 8110 LCR Meter

4.2 Physical dimensional characterization

The heterogeneous composition of compound thermoplastics causes surface roughness which may affect the quality of printing. The average surface roughness measured from 2D-profiles for the polycarbonate CDs used as substrate is 19.4 µm. This result compares well with the 19.3 µm 2D surface roughness measured for Epson photo paper [9], which is recommended as a standard substrate for the Dimatix printer. The surface roughness of the PC substrate is observable in Figure 8, which depicts the feature topography for an example dogbone section in the position where the line connects to the probe pad.

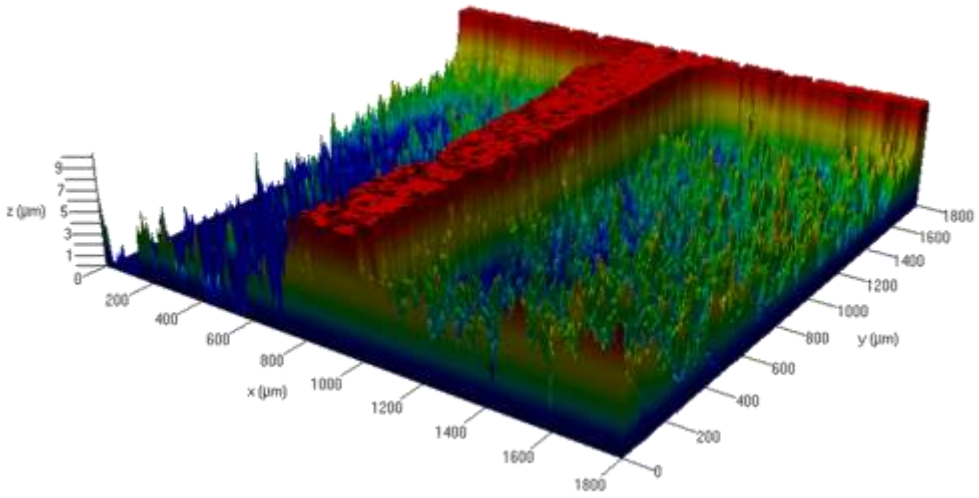

Figure 8 Example profile image of a 150 µm width printed line connecting to a pad

The averaged data extracted from the laser profilometry for the dog-bone structures of different drawn widths is presented in Table 5 and Table 6 for the width and thickness of the lines respectively.

Table 5: Laser profilometry line width results

Drawn width (µm)	*Print width spots* (number)	*Width result* (µm)	*Width variance* (%)	*Width spreading* (%)
150	6	252	50	168
500	20	574	6	115
1000	40	1100	2	110
1500	60	1560	2	104
2000	80	2130	2	106

Width spreading is defined as the width ratio of the printed to the drawn lines. Features are printed with overlapping jetted spots of size 80 µm at a spot spacing of 25 µm. Lines with a drawn width requiring the printing of only a few spots are expected to display significant spreading in the printed line width. The experimental results of the width indeed indicate that with increasing line width there is less spreading, and more accurate line widths can be printed with better precision.

Table 6: Laser profilometry line thickness results

Drawn width (µm)	*Thickness result* (µm)	*Thickness variance* (%)	*Surface roughness* (µm)	*Roughness variance* (%)
150	4.1	97	10.7	25
500	4.73	177	14.7	14
1000	5.87	16	23.8	28
1500	5.35	150	28.6	18
2000	5.46	6	19.8	13

The expected thickness of the printed features is in the order of a few micrometers, which is approaching the 1 µm resolution limit of the confocal microscope. Further taking into account that the line thickness is expected to be smaller than the average substrate surface roughness, inaccurate and noisy measurements may be anticipated - as can actually be seen in the large variance values in Table 6. Nevertheless, reasonable trends can be extracted

from the measurement data. In fact, the average printed film thickness in Table 6 is convincingly close to the supplier specified thickness value of 4 μm, with the positive difference explainable by incomplete sintering and resin binder burn-off due to the low thermal curing temperature.

The difference in layer thickness with respect to the line width is explicable by the volume of ink deposited per unit dimension of the width, according to the number of overlapping spots printed in the line width. Figure 9 (a) shows this ink density calculated from the drawn width, where the 90% and 95% values of the asymptotic saturation value are also indicated. To a first order the ink density beyond the 95% point may be considered constant, and therefore also the ensuing printed layer thickness. From Figure 9 (a) it can be deduced that the layer thickness for line widths larger than approximately $w_t \approx 800$ μm may be presumed constant. The ink density calculated from the measured line widths shown in Figure 9 (b) exhibit a coarse saturating curve, while the variance bars for the measured layer thickness suggest that the accuracy of these measurements is not adequate to identify the expected saturated shape. No more than an inference can be made on a rudimentary level of a generally increasing trend in layer thickness with increasing line width.

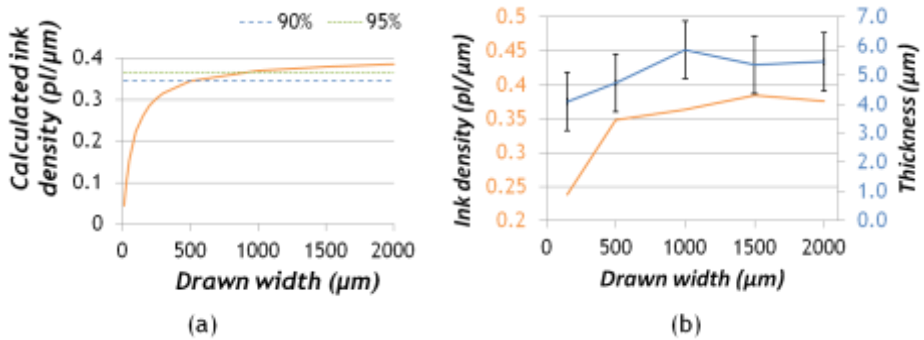

Figure 9 Comparison of (a) the ink density calculated with the drawn width and (b) the ink density calculated from the measured width, as well as the ensuing measured printed layer thickness

4.3 Electrical characterization

4.3.1 Frequency response

It ought to be confirmed that the impedance of tracks printed on polycarbonate has the expected high pass frequency response associated with a dominant series inductor as reactive component [9]. The LCR meter can measure the frequency response of several electrical parameters up to frequency of 10 MHz. The measured impedance magnitude spectrum for an example line in Figure 10 (a) clearly displays a high pass response, with a constant (resistive) value at lower frequencies, and a linearly proportional to frequency (inductive) value at higher frequencies. Figure 10 (a) also illustrates how the +3 dB point derived from circuit theory [15] may be used to extract the bandwidth of the track, the results of which is given in Figure 10 (b) for the different experimental track widths. The bandwidth values extracted from the frequency response measurements are approximately 30 times lower than those predicted by equation (4) of the model in Table 4, and also display large variance. The reason for this reduced bandwidth is related to higher than predicted inductance of the printed lines, and modeling and optimization of the inductance and frequency response will be pursued in further research. For the purposes of the current work, Figure 10 (b) indicates that the bandwidth of tracks remain above 1 MHz.

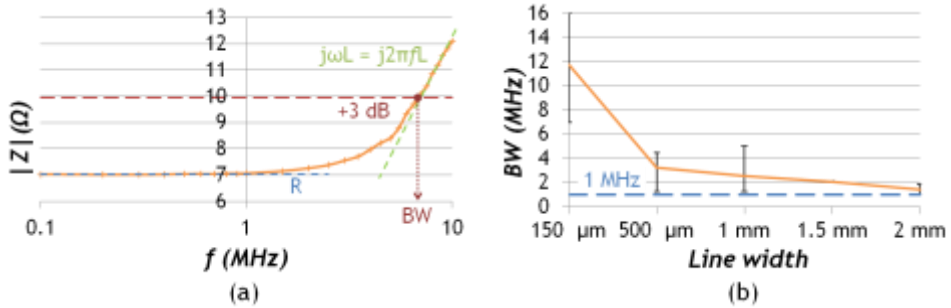

Figure 10 (a) Example measurement of the impedance spectrum (w = 150 µm, *l* = 8 mm) (b) extracted bandwidth for different line widths

4.3.2 Sheet resistance

Sheet resistance is indirectly proportional to the layer thickness, which in accordance with Figure 9 is expected to vary appreciably in the width region $w_t \leq 800$ µm. Because the layer thickness increases with increasing line width, this proportionality predicts a decreasing function of sheet resistance with respect to line width. The experimental results in Figure 11, though, reveal an increasing function of sheet resistance with respect to line width. There does appear to be an inflection point close to $w \approx 500$ µm, where the smaller slope for narrow lines may be explained by the dependence of sheet resistance on layer thickness - although the average variance of 17% renders such an interpretation indecisive. The increase in sheet resistance with respect to line width may be attributable to differences in sintering completion, and is probably related to the "coffee-ring" effect seen in Figure 6. For the purposes of comparison, features printed under similar conditions on polycarbonate CDs has equivalent thickness to those printed on Epson photo paper, but the average sheet resistance is an order of magnitude larger for the polycarbonate than for the paper [9]. Further investigation is required to produce methods for optimization. In the current work the linear regression analysis shown in Figure 11 yields a practical empirical model with a good R^2 coefficient of determination, which provides an acceptable sheet resistance parameter for simple electronic network design.

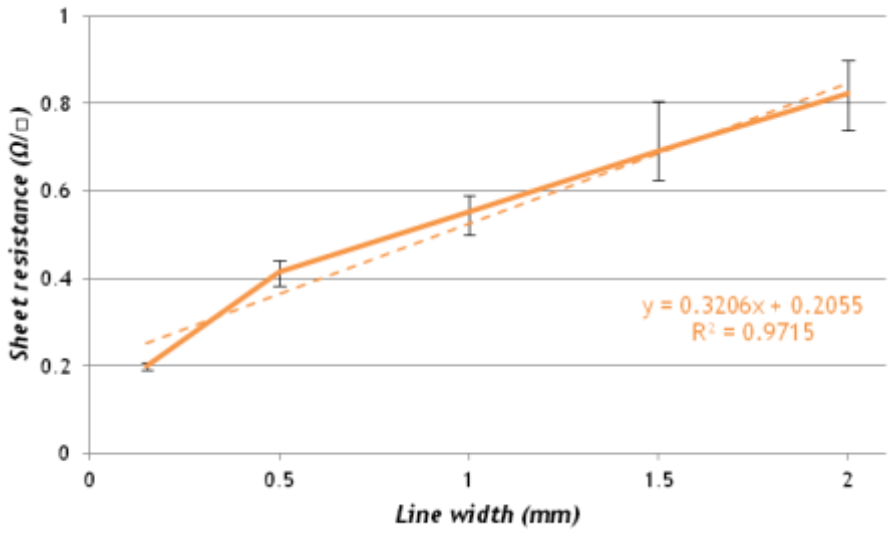

Figure 11 Sheet resistance for the track resistance model when length *l* = 8 mm

4.3.3 Design procedure

A systematic design procedure for reliably printing conductive networks on polycarbonate microfluidic CDs is represented in Figure 12. It is based mainly on the sheet resistance model of Section 4.3.2, while also including the theoretical inductance and bandwidth model equations of Section 3.2. The latter parameters will be refined with further research, but the design procedure - along with the manufacturing protocol defined in section 2 - yields electronic circuits operating resistively within a limited a bandwidth.

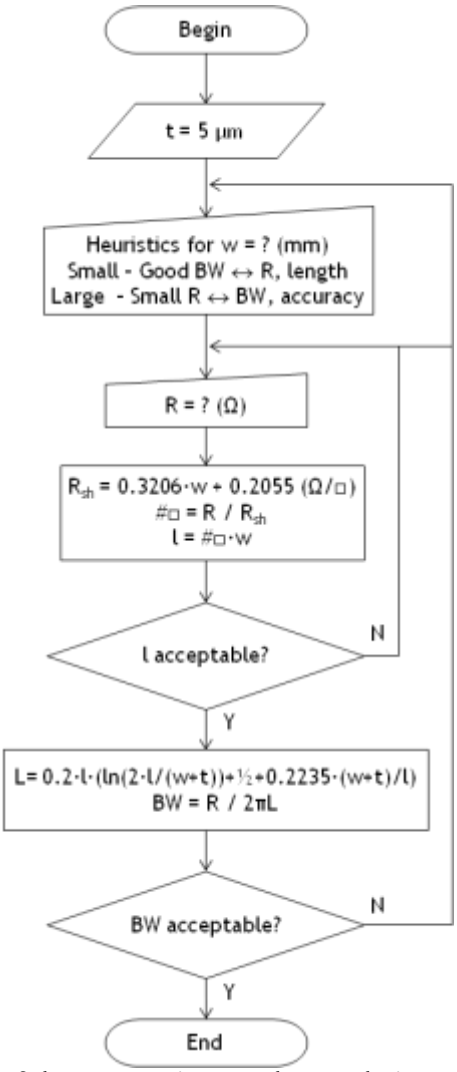

Figure 12 Flow diagram of the systematic procedure to design printed conductive tracks on polycarbonate CDs

4.3.4 Validation

The measured resistance and inductance is compared with the predicted values from the design procedure in Figure 12 for two sets of the test structures of Figure 3. The resistance results are graphed in Figure 13 (a), while Figure 13 (b) presents the inductance results. The variance of both resistance and inductance is 16% on average, but the worst case for resistance is 19%, while a worst case of 32% exists for inductance.

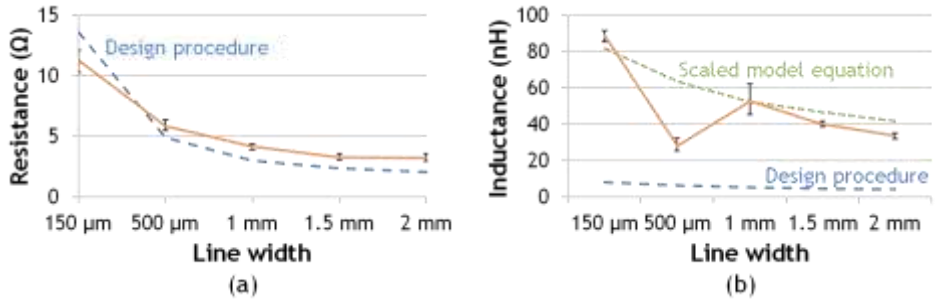

Figure 13 Measurements for the track model compared to the predicted values from the design procedure (*l* = 8 mm): (a) resistance (b) inductance

The model is further validated against a set of data generated from measurements of features fabricated on 5 different substrates in 3 printing runs. The data covers the width design space between 100 µm and 2 mm, and a length design space between 8 mm and 400 mm, with ensuing resistance values between 2 Ω and 275 Ω. The results predicted by the empirical model are generally within ± 30%, which is acceptable given the variance in data on which the model is based. The model is adequate for the purposes of a first design iteration for rapid prototyping.

5. EXTRACTED DESIGN RULES

New design rules are needed for design and simulation of printed electronics applications, and the rules given in Table 7 are extracted from the measured dimensional results for features printed on polyacarbonate CDs.

Table 7: Extracted design rules for printed features on polycarbonate CD substrates

Parameter	*Design rule*
Minimum width	80 µm
Maximum width	2000 µm
Minimum spacing	100 µm

6. CONCLUSION

Manufacturing biosensors on microfluidic materials require low-cost technologies and materials, which can yield reproducible and robust devices rapidly. The results obtained in this work contribute towards the research for fully printable rapidly prototyped electronic systems in smart ubiquitous biosensing, which require sensitive and robust signal readout at low power and low cost, with wireless connectivity to the Internet-of-Things (IoT) [8][16].

Apart from supporting rapid biosensor prototyping, printed electronics for biosensors provide an avenue for commercializing biomedical applications of nanomaterials, and promise to do so with high reliability, reproducibility and uniformity [16]. Although it is acknowledged that the translation from a demonstration-of-principle in a laboratory to a finished, manufactured, quality controlled, registered, distributed product is difficult and complicated, this work demonstrates conductive features successfully printed on polycarbonate – the substrate most often used in centrifugal CD-based microfluidics. A complete workflow is presented that enables the prototyping of printed electronics circuit networks for smart quantitative and sensitive CD-based microfluidics devices within one day.

Research is continuing to model the track inductance, which will offer a refined design procedure where the bandwidth will be more predictable and better controlled. The current lumped approximation electrical model can be extended to a more accurate

distributed model [17]. Another electrical parameter of interest is the current carrying ability of printed tracks, in order to investigate power dissipation limitations.

In future the polycarbonate surface activation processing may be improved, for example, PC is a thermoplastic that responds well to gas plasma treatment. Furthermore, mechanical parameters such as bending radius and lift-off may be investigated. Feauture design may be simplified with more uniform layer thickness and sheet resistance, requiring better control of the printed ink density, as well as the thermal sintering process. This work may also be extended by considering other sintering methods - more amenable to polymer substrates - than the recommended thermal sintering. Promising alternative sintering methods are infrared-assisted [18], plasma-assisted [19],electrically assisted [20], or photonic sintering, which includes laser-induced [21] techniques, as well as ultraviolet methods [22].

REFERENCES

[1] **Maxwell, E. J., Mazzeo, A. D. & Whitesides, G. M.** 2013. Paper-based electroanalytical devices for accessible diagnostic testing, *Materials Research Science Bulletin,* 4(38), pp. 309-314.

[2] **Cooksey, G. A. & Atencia, J.** 2014. Pneumatic valves in folded 2D and 3D fluidic devices made from plastic films and tapes, *Lab on Chip*, 14, pp. 1665-8.

[3] **Hugo, S., Land K., Madou M. & Kido H.** 2014. A centrifugal microfluidic platform for point-of-care diagnostic applications, *South African Journal of Science*, 110(1/2), #2013-0091.

[4] **Ahn, J. H. & Je, J. H.** 2012. Stretchable electronics: materials, architectures and integrations, *Journal of Physics D: Applied Physics, 4*5(10), #103001.

[5] **Zheng, Y., He, Z., Gao, Y. & Liu, J.** 2013. Direct Desktop Printed-Circuits-on-Paper flexible electronics, *Nature Scientific reports* 3, #1786.

[6] **Zheng, G., Cui, Y., Karabulut, E. Wågberg, L., Zhu, H. & Hu, L.** 2013. Nanostructured paper for flexible energy and electronic devices, *Materials Research Society (MRS) Bulletin,* 38(4), pp. 320-325.

[7] **Steckl, A.** 2013. Circuits on cellulose, *IEEE Spectrum,* 2(48), pp. 48-61.

[8] **Vena, A., Sydanheimo, L.,Tentzeris, M. M. & Ukkonen, L.** 2015. A Fully Inkjet-Printed Wireless and Chipless Sensor for CO2 and Temperature detection, *IEEE Sensors Journal*, 15(1), pp. 89-9.

[9] **Joubert, T-H., Bezuidenhout, P. H., Chen, H., Smith, S., Land, K. J.** 2015. Inkjet-printed silver tracks on different paper substrates, 7th International Symposium On Macro- and Supramolecular Architectures and Materials (MAM-14), Nov. 2014, Johannesburg, South Africa, Materials Today: Proceedings, 2(7), pp. 3891-3900

[10] **Ghaffarzadeh, K.** 2013. *Conductive Ink Markets 2013-2018: Forecasts, Technologies, Players*, IDTechEx Market Report.

[11] **Jankowski, P., Ogonczyk, D., Kosinski, A., Lisowski, W, & Garstecki, P.** 2011. Hydrophobic modification of polycarbonate for reproducible and stable formation of biocompatible microparticles, *Lab on Chip*, 11, pp. 748–752.

[12] **Kuhn, W. B. & Ibrahim, N. M.** 2001. Analysis of current crowding effects in multiturn spiral inductors, *IEEE Trans. Microw. Theory Tech*, 49(1), pp. 31–38.

[13] **Botha, T-H. & Du Plessis. M**. 1989. Technological design considerations of passive and non-MOS active components for analogue CMOS circuits, *South African Journal of Science*, 85, pp. 701-3.

[14] **Terman, F.E.** 1945. Radio Engineering Handbook, *McGraw-Hill*.

[15] **Horowitz, P. & Hill, W.** 1979. The Art of Electronics, *Cambridge University Press*, ISBN 978-0521231510.

[16] **Vyas, R., Lakafosis, V., Lee, H., Shaker, G., Yang, L., Orrechini, G., Traille, A., Tentzeris, M. M. & Roselli, L.** 2011. Inkjet printed, self powered, wireless sensors for environmental, gas, and authentication-based sensing, *IEEE Sensors Journal*, 11(12), pp. 3139-52.

[17] **Tang, K. T. & Friedman, E. G.** 2000. Lumped versus distributed RC and RLC interconnect impedances, *Proceedings of IEEE MWSCAS*, pp. 16–9.

[18] **Denneulin, A., Blayo, A., Neuman, C. & Bras, J.** 2011. Infra-red assisted sintering of inkjet printed silver tracks on paper substrates, *Journal Nanoparticle Research*, 13(9), pp. 3815–3823.

[19] **Reinhold, I., Hendriks, C. E., Eckardt, R., Kranenburg, J. M. Perelaer, J., Baumann, R. R. & Schubert, U. S.** 2009. Argon plasma sintering of inkjet printed silver tracks on polymer substrates, *Journal of Material Chemistry*, 19(21), p. 3384.

[20] **Hummelgård, M., Zhang, R., Nilsson, H-E. & Olin, H.** 2011. Electrical sintering of silver nanoparticle ink studied by *In Situ* TEM probing, *PLoS One*, 6(2), p. e17209.

[21] **Maekawa, K., Kawasaki, K., Niizeki, T., Mita, M., Matsuba, Y., Terada, N. & Saito, H.** 2012. Drop-on-demand laser sintering with silver nanoparticles for electronics packaging, *IEEE Transactions on Components, Packaging and Manufacturing Technology*, 2(5), pp. 868–877.

[22] **Polzinger, B., Schoen, F., Matic, V., Keck, J., Willeck, H., Eberhardt, W. & Kueck, H.** 2011. UV-sintering of injet-printed conductive silver tracks, *Proceedings IEEE Conference on Nanotechnology*, Portland, Oregon, pp. 201–204.